JOURNAL OF NEUROINFLAMMATION

RESEARCH Open Access

# Metabolic consequences of interleukin-6 challenge in developing neurons and astroglia

Jacquelyn A Brown[1,2†], Stacy D Sherrod[2,3†], Cody R Goodwin[2,4], Bryson Brewer[5], Lijie Yang[5], Krassimira A Garbett[1], Deyu Li[2,5], John A McLean[2,4], John P Wikswo[2,3,6,7*] and Károly Mirnics[1,2,8,9*]

## Abstract

**Background:** Maternal immune activation and subsequent interleukin-6 (IL-6) induction disrupt normal brain development and predispose the offspring to developing autism and schizophrenia. While several proteins have been identified as having some link to these developmental disorders, their prevalence is still small and their causative role, if any, is not well understood. However, understanding the metabolic consequences of environmental predisposing factors could shed light on disorders such as autism and schizophrenia.

**Methods:** To gain a better understanding of the metabolic consequences of IL-6 exposure on developing central nervous system (CNS) cells, we separately exposed developing neuron and astroglia cultures to IL-6 for 2 hours while collecting effluent from our gravity-fed microfluidic chambers. By coupling microfluidic technologies to ultra-performance liquid chromatography-ion mobility-mass spectrometry (UPLC-IM-MS), we were able to characterize the metabolic response of these CNS cells to a narrow window of IL-6 exposure.

**Results:** Our results revealed that 1) the use of this technology, due to its superb media volume:cell volume ratio, is ideally suited for analysis of cell-type-specific exometabolome signatures; 2) developing neurons have low secretory activity at baseline, while astroglia show strong metabolic activity; 3) both neurons and astroglia respond to IL-6 exposure in a cell type-specific fashion; 4) the astroglial response to IL-6 stimulation is predominantly characterized by increased levels of metabolites, while neurons mostly depress their metabolic activity; and 5) disturbances in glycerophospholipid metabolism and tryptophan/kynurenine metabolite secretion are two putative mechanisms by which IL-6 affects the developing nervous system.

**Conclusions:** Our findings are potentially critical for understanding the mechanism by which IL-6 disrupts brain function, and they provide information about the molecular cascade that links maternal immune activation to developmental brain disorders.

**Keywords:** glycerophospholipid, immune activation, interleukin, kynurenine, metabolomics, microfluidics, ultra-performance liquid chromatography - ion mobility - mass spectrometry

## Background

Maternal immune activation (MIA) strongly contributes to the pathophysiology of multiple brain disorders in the offspring, including schizophrenia [1], autism [2,3], major depression [4] and multiple sclerosis [5]. Importantly, mounting evidence suggests that altered immune status is not merely a reaction to a primary disease process, but an etiological contributor to the disease itself [6,7]. It has been well documented that disturbed cytokine levels can cause long-term behavioral changes. For example, in animal models, maternal infection with influenza virus during pregnancy leads to long-lasting microanatomical, neurochemical, and behavioral changes in the brains of the offspring [8,9]. However, such changes are not mediated directly by the viral infection [10]. Rather, MIA appears to be the key [11], as offspring of mothers exposed to polyinosinic:polycytidylic acid (polyI:C, a synthetic

* Correspondence: john.wikswo@vanderbilt.edu; karoly.mirnics@vanderbilt.edu
†Equal contributors
[2]Vanderbilt Institute for Integrative Biosystems Research and Education, 6809 Stevenson Center, Vanderbilt University, Nashville, TN 37235, USA
[1]Department of Psychiatry, 465 21st Avenue South, Vanderbilt University, Nashville, TN 37232, USA
Full list of author information is available at the end of the article

cytokine-inducing immunostimulant) show deficits similar to those of offspring whose mothers were exposed to virus infection [12].

MIA triggers a complex immune response that ultimately alters the developmental trajectory of the fetal brain [9]. Cytokines play a critical role in MIA, and in particular, interleukin-6 (IL-6) induction appears to be responsible for many of the long-lasting behavioral changes seen in MIA-born offspring [13,14]. IL-6, a pro-inflammatory cytokine with a profound effect on brain function [15,16], is elevated as a result of various MIA paradigms, and exposure to IL-6 gives rise to a similar behavioral phenotype that is observed in offspring of mothers exposed to flu, lipopolysaccharide (LPS), or polyI:C [12-14]. Furthermore, blocking IL-6 effects with anti-IL-6 antibody during influenza-virus infection, polyI:C exposure, or IL-6 challenge prevents the deleterious effects of MIA [13], thus suggesting that the IL-6 inflammatory cascade is a critical (and at least partially causal) mediator of the deleterious effects observed in the offspring.

Within the central nervous system, cells communicate through multiple mechanisms, including synaptic contacts, active secretion of proteins, and release of metabolites. The non-synaptic communication between the various brain cell types is extremely important during development, and the various chemical gradients are critical for brain patterning, neuronal differentiation and migration, laminar development and establishment of the synaptic framework [17]. Thus, the ability to study the molecular secretions in the developing brain in a high-throughput, unbiased way provides insight into typical fetal brain development and pathological processes that result in developmental disorders. Custom-made, microfabricated bioreactors (such as microfluidic chambers) offer the opportunity to maintain tissue explants and small numbers of primary cells in a close-to-physiological environment, wherein the extracellular volume and fluid interconnectivity between cellular compartments are sufficiently optimized for studying paracrine and autocrine signaling phenomena without dilution [18,19]. This, coupled with ultra-performance liquid chromatography - ion mobility - mass spectrometry (UPLC-IM-MS), provides an opportunity to study the exometabolomic features of numerous cell types under tightly controlled conditions [20] and with narrow temporal resolution.

Considering these strengths, we have applied microfluidic-based culturing of embryonic neurons and glial cells to study their exometabolomic activity under resting conditions and upon stimulation with interleukin-6. In a comprehensive comparison of baseline and IL-6-induced changes across these two cell types, we putatively identified metabolites and molecular pathways that might play a critical role in the pathophysiology of neurodevelopmental disorders.

## Methods

### Experimental animals

C57 black male and female mice were kept in mating for 3 days. E0 was defined as time of vaginal plug. At E15 pregnant females were euthanized with isofuran overdose and embryos removed. The ventral midbrain was isolated as previously described [21]. All procedures were in accordance with IACUC standards and were approved by Vanderbilt's Institutional Animal Care and Use Committee for use in this study.

### Neuronal and astroglial cell cultures

Neuronal cultures were prepared as previously described using Hibernate-E dissection media [22]. The ventral midbrain of each E15 embryo was dissociated in Hank's balanced salt solution (HBSS) containing 1% papain and 5 U $mL^{-1}$ DNase (Worthington Biochemicals, Lakewood, NJ, USA) and transferred to a solution containing 1% ovomucoid protease inhibitor (Worthington Biochemicals, Lakewood, NJ, USA). After dissociation, neurons and astroglia were separated by magnetic cell sorting using established protocols [23]. Dissociated cells were immuno-enriched using a PNCAM antibody (Miltenyi Biotec, Bergisch Gladbach, Germany), thus positively selecting for neurons and allowing astroglia to be collected in the flow-through. This purification method achieved approximately 94% purity in cell culture. Following centrifugation, purified neurons were resuspended in neural basal (NB) culture media (supplemented with B-27 and 2 mM L-glutamine) and loaded into poly-D-lysine (10 μg $ml^{-1}$) and laminin (9.6 μg $ml^{-1}$)-coated microfluidic chambers. Primary astrocyte cultures were reconstituted and maintained in minimum essential medium (MEM) (supplemented with 10% albumin and N-2) for 3 days. On day 4, cell culture media was exchanged for NB culture media (supplemented with B-27 and 2 mM L-glutamine) for the following 3 days [24-26]. Microfluidic chambers were loaded with approximately 200,000 cells/well and cell cultures were maintained at a constant gravity-fed flow for 6 days prior to exposure.

### Exposure to IL-6

On the $6^{th}$ day, the above-described culturing media was replaced with media containing 100 ng $ml^{-1}$ IL-6 (Shenandoah Biotech, Warwick, PA, USA) for 2 hours. Following media replacement, effluent was collected for 2 hours, collecting a total flow-through volume of 60 μl/sample. Three biological replicates for each condition were collected. (*Experimental conditions*: Neuronal cultures, Neuronal cultures + IL-6, Astroglial cultures, Astroglial cultures + IL-6; *Controls:* Empty microfluidic chamber containing no cells, Empty microfluidic chamber no cells + IL-6). Each UPLC-IM-MS measurement was performed in triplicate (technical replicates).

### Microfluidic chambers

Microfluidic devices were fabricated using standard soft lithography methods [27,28] as previously described [29-31]. First, a master mold was formed using a negative SU-8 photoresist. Spin-coating SU-8 2100 (Microchem, Newton, MA, USA) on a silicon wafer at 1500 RPM resulted in a uniform layer of photoresist approximately 200-μm thick. Standard photolithographic methods were used to pattern the desired microchannel features into the SU-8. Briefly, the SU-8 film was exposed to UV light through a 20,000 DPI printed transparency mask (CAD-Art, Bandon, OR, USA), baked for 2 hours at 95°C, and processed with SU-8 developer to yield a 3D relief of the 2D pattern on the mask. After fabrication of the mold, liquid polydimethylsiloxane (PDMS) prepolymer (Dow Corning, Midland, MI, USA) was mixed with its curing agent (10:1 ratio) and poured over the mold. The PDMS was then degassed for approximately 1 hour and cured in a 70°C oven for at least 2 hours. Following curing, the PDMS layer was removed from the SU-8 mold, and 5-mm diameter holes were punched in the inlet and outlet of each microfluidic channel. Air plasma bonding was then used to attach the PDMS layer to a glass cover slip (VWR Vista Vision, Suwanee, GA, USA). After bonding, Pyrex cloning cylinders (Fisher Scientific, Pittsburgh, PA, USA) were adhered to the inlet/outlet regions of each channel to form small reservoirs to load and remove cells and culture media. Prior to use, individual microfluidic channels were stored in deionized water.

Microfluidic devices consisted of four separate microchannels, each having an inlet and outlet channel and one cell culture chamber region (Figure 1A). The devices were designed to reduce flow velocity by expanding the cell culture chamber. The larger cell culture chamber, with dimensions of 5,400 μm (*length*) × 800 μm (*width*) × 200 μm (*height*), facilitates cell attachment and has a total volume of approximately 0.86 μL. A PDMS wall separates the four chambers, ensuring that no cross talk occurs among cell culture regions.

### Sample preparation for mass spectrometry

Metabolites were prepared for ion mobility - mass spectrometry (IM-MS) analysis by concentrating *in vacuo* (SpeedVac concentrator, Thermo-Fisher) and reconstituting in 60 μL of 90% acetonitrile, 10% $H_2O$, and 20 mM ammonium acetate (pH = 9). Quality control samples were prepared by combining equal volumes (15 μL) of each sample type.

### Mass spectrometry and data analyses

UPLC-IM-MS and data-independent acquisition ($MS^E$) were performed on a Waters Synapt G2 HDMS (Milford, MA, USA) mass spectrometer equipped with a Waters nanoAcquity UPLC system and autosampler (Milford, MA, USA). Metabolites were separated on a 1 mm × 100 mm

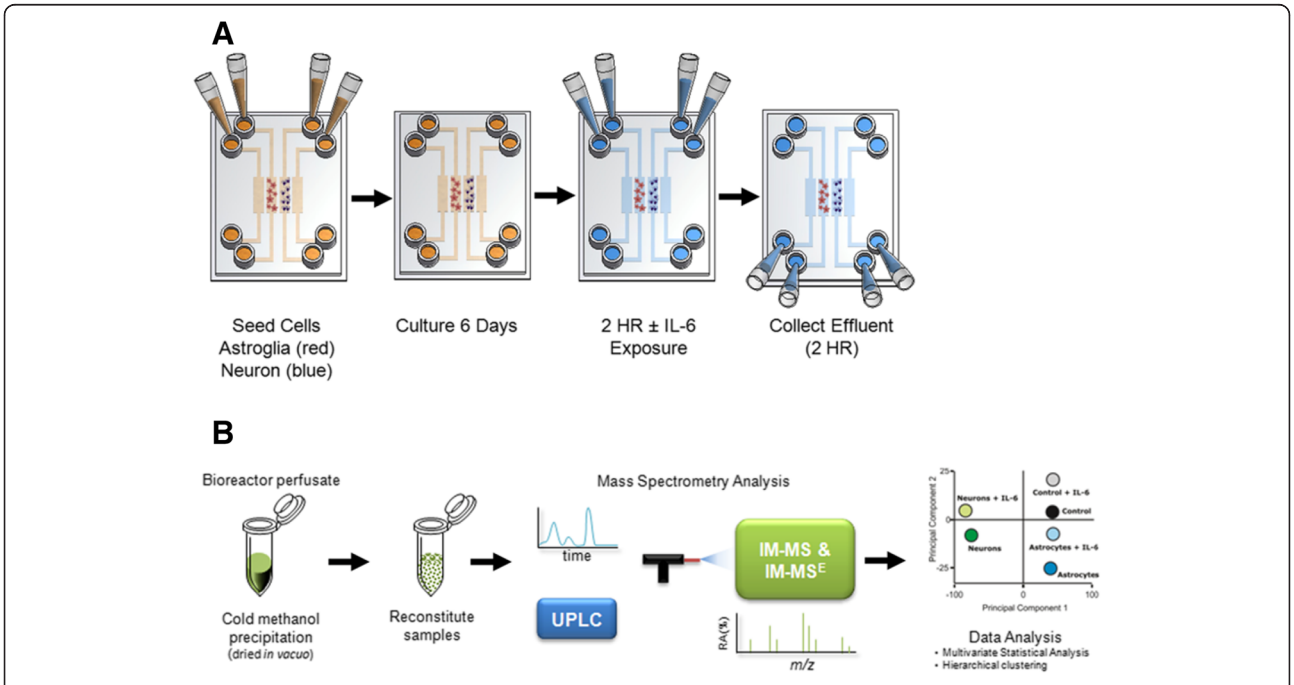


**Figure 1 Experimental design and analysis strategy. (A)** Microfluidic devices or bioreactors were seeded with neurons or astroglia for 6 days prior to IL-6 exposure. **(B)** Illustration of the sample preparation method for bioreactor perfusate samples (control ± IL-6, astroglia ± IL-6, and neurons ± IL-6). Samples were prepared for exometabolomic analyses and analysis performed using an ultra-performance liquid chromatography-ion mobility-mass spectrometer.

hydrophilic interaction column packed with 1.7-μm, 13-nm ethylene bridged hybrid (BEH) particles (Waters, Milford, MA, USA). Liquid chromatography was performed using a 20-minute gradient at a flow rate of 90 μL $min^{-1}$ using solvent A (10% $H_2O$ (v/v) with 10 mM ammonium acetate at pH 9 in acetonitrile) and solvent B (100% $H_2O$ with 10 mM ammonium acetate at pH 9). A 3-min wash period (99% solvent A) was performed prior to any gradient changes. After 3 min, solvent B increased to 75% over 12.5 min and up to 50% in 15 min. The column was re-equilibrated to 99% solvent A for 5 min after each run. Typical IM-MS analyses were run using resolution mode, with a capillary voltage of 3.5 kV, source temperature at 120°C, sample cone at 5, source gas flow of 400 mL $min^{-1}$, desolvation temperature at 400°C, He cell flow of 180 mL $min^{-1}$, and an IM gas flow of 90 mL $min^{-1}$. The data were acquired in positive ion mode from 50 to 1700 Da with a 0.3 s scan time; full-scan data were mass corrected during acquisition using an external reference consisting of 3 ng $mL^{-1}$ solution of leucine enkephalin infused at a flow rate of 7 μL $min^{-1}$. All analytes were analyzed using $MS^E$ with an energy ramp from 10 to 45 eV.

### Data analysis

The integrated intensity of each chromatographically resolved m/z peak was $log_2$ transformed. Differences in these peak areas were determined using the average logarithmic ratio ($ALR = mean_{EXP} - mean_{CNTR}$). Statistical significance was determined using unpaired two-tailed Student's t-test. Both biological and technical replicates were used in these calculations. An m/z species was considered differentially expressed when it met the dual criteria of absolute value $|ALR| > 0.585$ (50% change) and $P$ value <0.05. Direction of change was defined as ALRs >0.585 = produced ALRs < -0.585 = consumed. The $log_2$ peak area values of species with differential levels between the experimental and control samples were subjected to a two-way unsupervised hierarchical clustering analysis based on Euclidian distance using GenePattern software [32].

### Identification of analytes by ion mobility - mass spectrometry

The raw data acquired were converted to mzXML files using ProteoWizard msconvert [33]. Following conversion, mzXML files were analyzed using XCMS in the statistical package R Studio (v 0.97.449) to pick and align features (that is, retention time (RT) - mass-to-charge (*m/z*) ratio pairs). XCMS was used with default settings except for rector (method = 'obiwarp'). Data were then normalized to the summed total ion intensity per chromatogram, with the total ion count normalized to 10,000 counts. The resulting processed data matrix was introduced into uMetrix (Version 2.0.0) EZ Info multivariate statistical analysis software for principal component analysis (PCA) with Pareto scaling.

Metabolite peak identifications were putatively assigned using both accurate mass measurements and MS/MS analysis. Ion mobility separations were utilized to isolate precursor ions, correlate product ions, and discern in-source fragmentation. Candidate structures were obtained and interpreted with available biochemical databases, including METLIN [34], the Human Metabolome Database [35], and LIPID MAPS [36] [see Additional files 1, 2, 3, 4 and 5].

### Determination of metabolomics differences

Principal component analysis was performed on expression levels of all measurable analytes using uMetrix (v 2.0.0) EZ Info extended statistics software. Unsupervised, two-way hierarchical clustering (samples versus analytes) was performed on normalized $log_2$ analyte levels in GenePattern [32] using Pearson distance. To determine differentially expressed analytes, all analyses were performed on log2-transformed values. Analytes were considered differentially expressed if they met a dual set of criteria of magnitude change and significance ($P$ <0.05; $|ALR| > 0.585$). Additionally, for an analyte to be changed under IL-6 stimulation, it also had to be significantly different ($P$ <0.05) from the IL-6 media perfused through the microfluidic chamber containing no cells. These calculations were performed in MS-Excel 2010.

## Results

### Resting astroglia and neurons exhibit distinct metabolic signatures

To investigate the resting-state metabolic signatures of astroglia and neurons, these cells were isolated from E15 mouse embryos using magnetic beads and cultured for 6 days in microfluidic chambers (Figure 1A). On day 6, we collected conditioned media from neuronal and astroglial cells, and as a control, media was perfused through the microfluidic device that contained no cells. Each conditioned media was prepared and analyzed by UPLC-IM-MS (Figure 1B). Following data processing (peak picking and alignment), 2,295 unique features (with each feature having both a mass-to-charge ratio (m/z) and a retention time (RT)) were detected [see Additional file 6: Dataset 1]. To enable study of the metabolic signatures and differences between cell types, the area of each UPLC-IM-MS peak from media for each cell type (neurons and astroglia) was compared to the same features in control media using a paired t-test. In this analysis, 14% (327) of the detectable exometabolites reported significantly different levels ($P$ <0.05) between neuronal cultures and control conditions. In contrast, 99% (2,278) of the detectable exometabolites were present at significantly different levels ($P$ <0.05) between astroglia and matched controls.

Of the 2,278 statistically significant chemical species, 1,576 (69%) were at lower levels in astrocyte-conditioned media than in the control media (three downward arrows in the astrocyte circle in Figure 2A), consistent with the astroglia metabolizing the associated chemical species provided by the original media. For the astroglial media, increased levels of 702 features (31%) relative to the control are indicated by upward arrows and represent production of these species by the astroglia. In contrast, neurons consumed 62 (19%) and produced 265 (81%) species.

However, it is noteworthy that the exometabolic activity observed in neurons showed a large overlap with the species observed in astroglia: of the 327 species consumed or produced by neurons, 310 (94.8%) were common to both the astroglial and neuronal media, with 289 (93.2%) of these showing the same directionality of changes (Figure 2A). We hypothesize that this common neuronal-astroglial exometabolic signature reflects basic homeostatic activity such as glucose utilization, mitochondrial function, and basic protein/lipid turnover.

Next, to directly compare the levels of astroglial species with the neuronal ones, we used a combined paired t-test and magnitude-change criteria applied to the average $\log_2$ ratio (ALR), such that $P < 0.05$ AND $|\text{ALR}| > 0.585$, which selects only species with a >50% difference. Of the original 2,278 species, 872 species met both criteria and revealed that astroglia produced approximately 15× more metabolites than neurons (astroglia = 824, neurons = 48) [see Additional file 7: Dataset 2].

For all technical and biological replicates and each of the 872 species, we computed the deviation of the astroglial and neuronal levels of each sample from the combined mean of that species for all samples. This created a matrix of 872 × 18. We then performed a two-way unsupervised hierarchical clustering on this matrix to produce the self-organized data in Figure 2B. The deviation from the mean was color-coded (red > mean, blue < mean), with the intensity of each color proportional to the magnitude of that deviation. This analysis demonstrates the technical and biological reproducibility of the measurements of these 872 species, and that the unsupervised clustering separates the species by the cell type that conditioned the media. Hence, our data suggest that astroglia and neurons have distinct metabolic signatures under resting conditions, while astroglia have a robust consumption/production metabolic activity and neurons consume/produce fewer metabolites in their resting state.

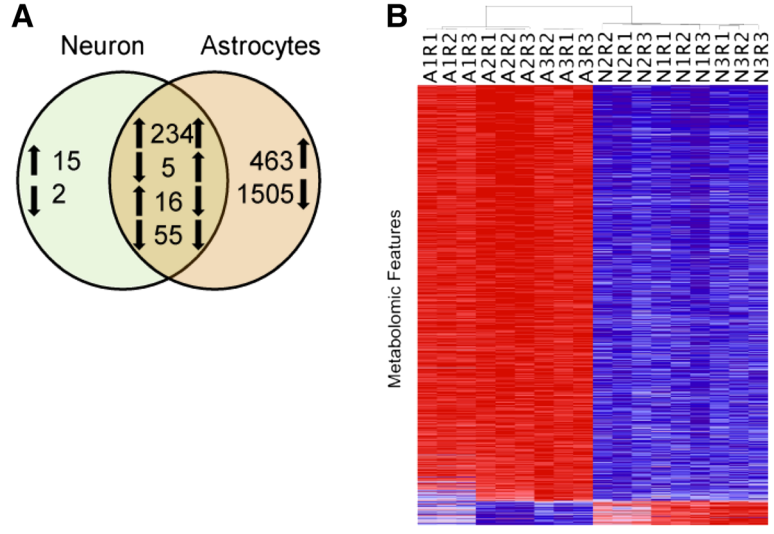


**Figure 2 Unstimulated neurons and astrocytes have a distinct exometabolomic profile. (A)** Venn diagram illustrating the number of features with significant differences between neurons versus control, and astrocytes versus control ($P < 0.05$). Numerals denote the number of analytes reporting significantly different levels, while arrows denote directionality of change in comparison to controls (perfused chambers containing no cells). Note that the astrocytes show much higher metabolic activity than neurons, and that 94.8% of the changed neuronal metabolites are also observed in cultured astrocytes. Of the 2,278 species detected in the astrocyte-conditioned media, 69% were consumed, as compared to 19% in the neuronal media. **(B)** Clustering of unstimulated astrocytic and neuronal exometabolomic profiles. Heat map shows two-way unsupervised hierarchical clustering analysis of normalized metabolomics data for the features observed in astrocytes and neurons in their unstimulated state after subtraction of the peak areas for control media (for analytes, [see Additional files 6, 7, 8 and 9]). Columns represent biological and technical replicates (for example, A1R1 - astroglia biological replicate 1 technical replicate 1), rows represent individual chemical species identified by the ultra-performance liquid chromatography - ion mobility - mass spectrometry (UPLC-IM-MS). In individual features, red denotes higher metabolite production in comparison to the other cell type. Note that higher metabolite production was the predominant feature of the astrocytic cultures, and that the clustering separated the biological and technical replicates into two distinct neuronal and astroglial clusters.

### Metabolic signatures of neurons and astroglia in response to IL-6 challenge

To investigate the metabolic response of each cell type to pro-inflammatory cytokine stimulation, we cultured the isolated astroglia and neurons in microfluidic devices, and cultures were exposed to 100 ng $ml^{-1}$ IL-6 for 2 hours on day 6. Control cells were exposed to vehicle only, and the control device contained no cells but was perfused with media containing IL-6. To address the issue of toxicity for both IL-6 dose and exposure time, neuronal and glial cells ± IL-6 were imaged 1 hour after treatment using β3-tubulin antibody (TUJ-1, a neuronal marker) or glial fibrillary acidic protein (GFAP, astrocyte marker) staining. Assessments did not reveal any change in process length, cell density, or other morphological signs of toxicity (Figure 3A).

The extracellular metabolomic signatures of neuronal and astroglial samples were significantly altered in response to IL-6 stimulation [see Additional files 8 and 9]. In the neuronal cultures, we observed 27 metabolites that changed in response to IL-6 exposure, with nine features exhibiting increased abundances and 15 demonstrating decreased abundances [see Additional files 8 and 9]. The response of the astroglial cultures to IL-6 exposure was more pronounced; of the 45 changed species, 28 species reported increased exometabolomic abundances, while 17 species were observed at reduced levels in the media [see Additional files 8 and 9]. Importantly, the responses of neuronal and astroglial cultures to IL-6 stimulation were quite distinct (Figure 3B): the observed neuronal changes were dominated by exometabolome decreases, while the majority of the astroglial alterations were increases. It is also noteworthy that three secreted species were significantly different in both the neurons and astroglia when compared to non-IL-6 exposed cultures (*m/z* 664.291, RT = 232 s; *m/z* = 760.278, RT = 213 s; *m/z* 748.234, RT = 109 s), with all showing opposite directionality of change between the two cell types [see Additional files 8 and 9]. These data illustrate that the initial, narrow time window for metabolic response of astroglia to IL-6 stimulation was predominantly characterized by an increase in metabolite production, while neurons increased their metabolite consumption.

These data comparisons between neuronal cultures, astroglial cultures, and control conditions demonstrate the powerful capabilities of UPLC-IM-MS analysis without *a priori* knowledge. This is also demonstrated by a principal component analysis (PCA) that distills multi-dimensional data sets (in these data, approximately 2,300 m/z-RT pairs) to principal components that best describe the greatest covariance in the data, thus providing sample grouping or separation based on patterns in the data. Global PCA of processed UPLC-IM-MS data from neurons, astroglia, and controls further confirmed that the global metabolic signatures between neuronal and glial sample types were quite distinct (Figure 3C).

### Identification of selected analytes by ion mobility - mass spectrometry

Peak identifications were performed using accurate mass and ion adduct information for database searching (METLIN [34], LIPID MAPS [36], and the Human Metabolome Database [35]) to produce candidate structures. Candidate structures were then validated using retention time and ion mobility-filtered high-energy data. Fragmentation is performed after the mobility separation, and therefore, product ions retain the mobility of the precursor. This allows untargeted fragmentation of all ions to be filtered into relevant high-energy spectra.

From the prioritized list of metabolites altered by IL-6 exposure, we putatively identified three analytes (Figure 4A) that belong to the glycerophospholipid metabolism pathway (Figure 4B). The connection of this pathway to brain IL-6 activation has not previously been described. *N*-methylethanolamine phosphate was observed to be increased in the IL-6-exposed neurons (m/z = 156.065, RT = 314 s, ALR = 1.81, $P$ <0.001) in comparison to the sham-treated neuronal cultures. Baseline levels of *N*-methylethanolamine phosphate were significantly higher in the glial cultures compared to those observed in the neuronal cultures. *N*-methylethanolamine phosphate can be produced through the transfer of a methyl group from *S*-adenosyl methionine to phophoethanolamine, catalyzed by phosphoethanolamine methyltransferase. This metabolite has an important biological role in glycerophospholipid metabolism and in development [37]. Importantly, the production of at least two other glycerophospholipid metabolites was detected in the secreted metabolome of IL-6 stimulated astroglia: diacylglycerophosphocholine (m/z = 732.551, RT = 216 s, ALR = 1.57, $P$ <0.001) and diacylglycerophospho-ethanolamine (m/z = 768.564, RT = 124 s, ALR = 1.39, $P$ <0.001). Glycerophosphocholines are the inactive form of long-chain polyunsaturated fatty acids (LCPUFAs), arachidonic acid (AA), docosahexaenoic acid (DHA), and eicosapentaenoic acid (EPA), and the disturbed metabolism of these species has been previously linked to schizophrenia, major depression, and bipolar disorder [38-42].

In addition, in both neuronal and astroglial cultures we observed IL-6-induced exometabolome changes in the tryptophan-kynurenine pathway, a pathway strongly modulated by IL-6 activity in the brain. Kynurenine (m/z = 209.10, RT = 78 s) was observed to decrease in astroglial cultures in response to IL-6 exposure (Figure 5A, ALR = −0.86, $P$ <0.00001), whereas formylanthranilate (m/z = 166.07, RT =70 s) was observed to increase in neuronal cultures in response to IL-6 exposure (Figure 5B, ALR = 2.47, $P$ <0.001). Formylanthranilate is a

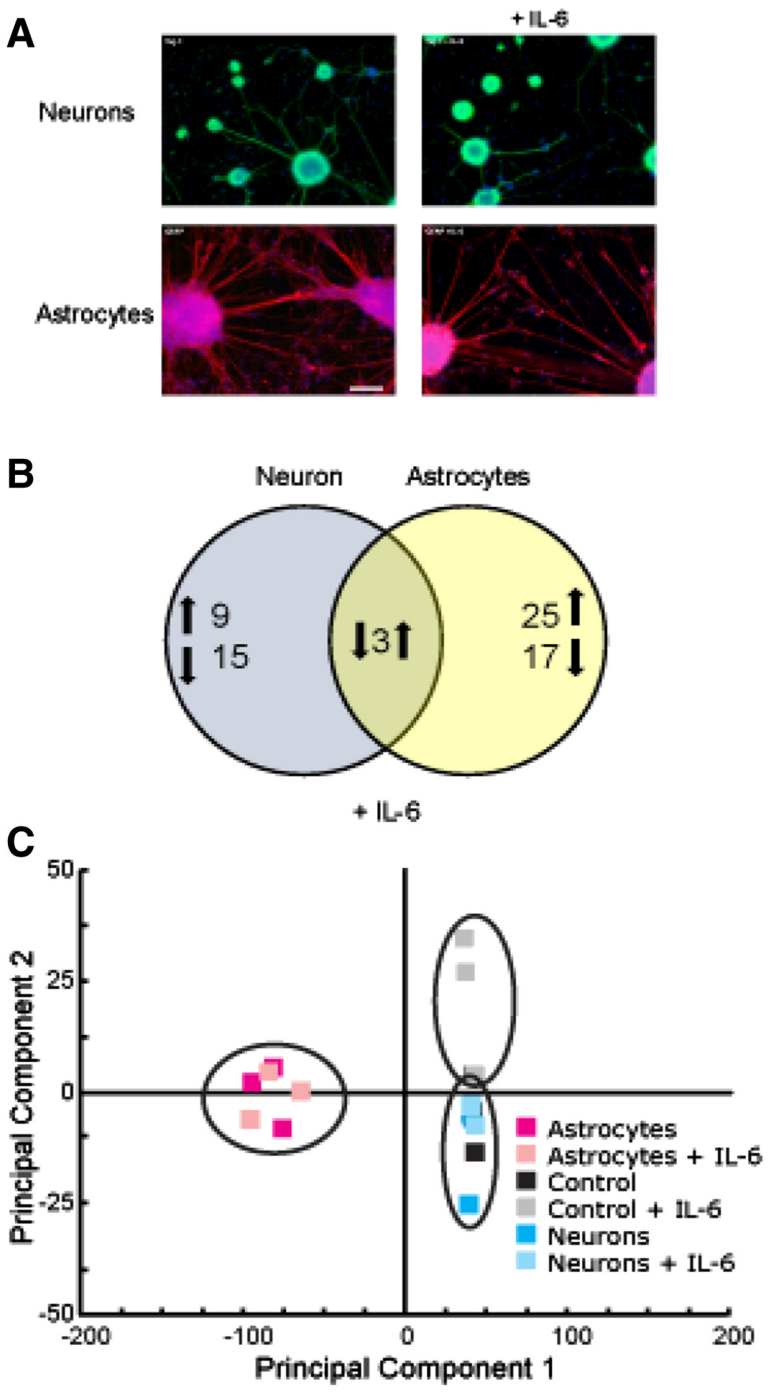


**Figure 3 Effects of IL-6 exposure on astrocytes and neuronal cultures. (A)** Cultured neurons and astrocytes were exposed to IL-6 for 2 hours and allowed to recover for 1 hour prior to imaging. Cells were fixed with 4% PFA and labeled with neuronal marker Tuj-1 or GFAP, an astrocyte marker. Appearance, process length, and cell density were similar to the untreated, matched controls. **(B)** Venn diagram illustrating the number of features with significant differences between IL-6 treatment and matched, sham-treated control cultures ($P$ <0.05; | ALR | >0.585, that is, >50% of control). Numerals denote the number of features ($m/z$ and retention time pairs) with significantly different levels, while arrows denote directionality of change in comparison to controls. Note that the neuronal and astroglial exometabolome response to IL-6 treatment is distinct. **(C)** Global principal component analysis (PCA) of ultra-performance liquid chromatography - ion mobility - mass spectrometry (UPLC-IM-MS) data illustrating that there are distinct metabolic signatures between neuronal and astroglial sample types.

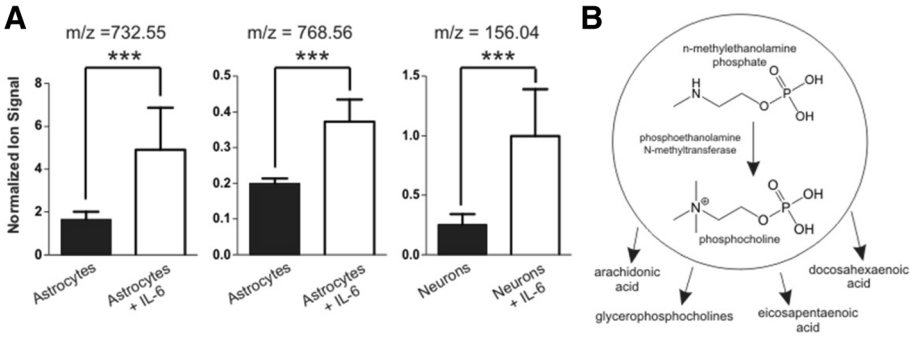


**Figure 4 Activation of glycerophospholipid metabolism in response to IL-6. (A)** Numerous glycerophospholipid metabolites were significantly produced upon IL-6 exposure in both astrocytes and neuronal cultures. Three analytes were putatively identified as diacylglycerophosphocholine (*m/z* 732.55, ALR = 1.57, *P* <0.001), diacylglycerophospho-ethanolamine (*m/z* 768.56, ALR = 1.39, *P* <0.001), and n-methylethanolamine (*m/z* 156.04, ALR = 1.81, *P* <0 .001). Putative identifications were obtained by using mass measurement accuracy, retention time and confirmed based on fragmentation spectra [see Additional files 1, 2, 3, 4 and 5]. **(B)** Illustrates a simplified glycerophospholipid metabolism pathway and shows that n-methylethanolamine is a precursor metabolite to numerous developmentally important downstream metabolites.

downstream metabolite in the kynurenine pathway that yields neuroactive intermediates and has implications in the modulation of neurotransmitter systems [43]. Importantly, both formylanthranilate and kynurenine are part of the tryptophan-kynurenine metabolic pathway, and disturbances of this pathway are considered common mediators of genetic and environmental effects in major depressive disorder [44] and appear to contribute to schizophrenia pathophysiology [41,45]. Taken together, these data suggest that glycerophospholipid metabolism and tryptophan-kynurenine metabolite secretions are important (and potentially related) metabolic pathways by which IL-6 inflammation affects the developing nervous system and predisposes it to developing a brain disease.

## Discussion

In traditional culture systems, cells are grown in a volume of media that is large enough to require media changes no more than once per day [46], often diluting

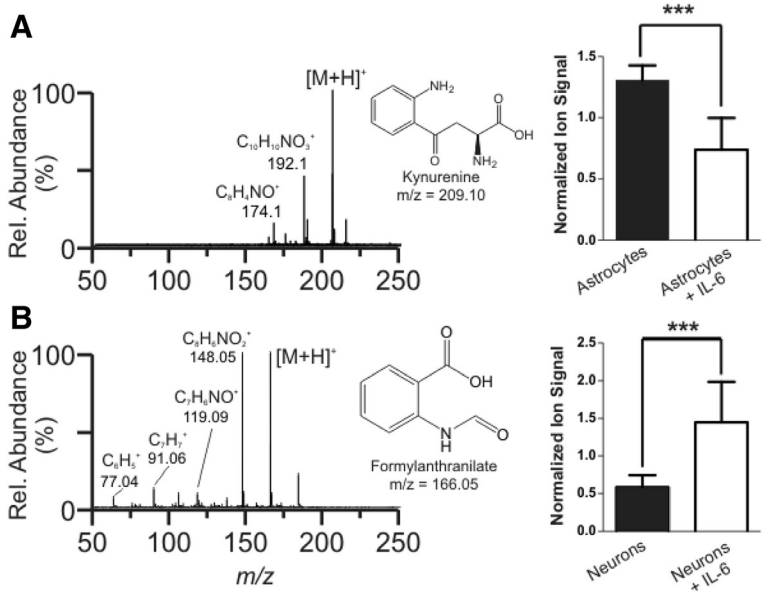


**Figure 5 Alterations to the kynurenine pathway after IL-6 treatment.** High energy (fragmentation) mass spectra for **(A)** *m/z* 209.10 (kynurenine) and **(B)** *m/z* 166.05 (formylanthranilate). Spectra were mobility separated to isolate only product ions for 209 and 166, respectively. **(A)** In astrocyte cultures, we observed a decrease in normalized ion signal after IL-6 treatment, ALR = −0.86, *P* <0.00001, for kynurenine (*m/z* 209.10). **(B)** In contrast, we observed an increase in ion signal for formylanthranilate (m/z 166.05), also a component of the kynurenine pathway, when neuronal cultures were treated with IL-6, ALR = 2.47, *P* <0.001. Taken together, these data show that IL-6 exposure alters both neurons and astrocytes but does so in an opposite manner.

the secreted molecules [47,48] to non-detectable levels [19]. Molecular signals can ostensibly be concentrated by prolonged culturing time, but at a cost of significant loss in temporal resolution. This is problematic, since cellular response to cytokine exposure is swift [49] and typical physiological effects of cytokines are characterized by rapid cycles [50]. To address these issues, we implemented a microfluidic culture chamber system with a 30-fold decrease in metabolite dilution when compared to conventional culture methods. This provided a means to increase temporal sampling resolution of the exometabolome, thereby utilizing the resultant increase in the sensitivity to changes in the concentrations of extracellular secretion. This increased sampling rate decreased the probability of analyte degradation and dilution over time. Furthermore, in the future it will allow investigators to perform continuous post-stimulation sampling in narrow time windows, opening the door to reconstruction of temporal cascades of metabolic activity.

Astroglia are well known to communicate with secreted molecules, and astrocyte-conditioned media has proven beneficial for neuronal growth and survival [47]. Thus, it is not surprising that astroglial cultures at baseline produce almost ten times more detectable analytes than neuronal cultures. An unexpected finding, however, was that resting astrocytes depleted the media of 1,576 analytes, or 69% of detected compounds. Identification of these consumed compounds and understanding the process of resource utilization will be important topics for future studies. It is also important to note that while the neurons enriched the conditioned media by only 15 detected analytes, we cannot exclude the possibility that these molecules are critical for neuronal-neuronal, neuronal-glial, or neuronal-microvascular communications [51].

The outcome of the IL-6 stimulation was perhaps the most interesting finding in our dataset. Neuronal and glial response to IL-6 stimulation was quite distinct, non-overlapping, and divergent: astroglia predominantly increased their metabolite production, while neurons primarily consumed resources from the media. We believe that these two metabolic signatures are parts of an essential chemical communication mechanism between neurons and glia under stress, and they perhaps represent an initial neuroprotective response to adverse conditions. In follow-up experiments, we were able to positively identify five distinct metabolites that were decreased in astroglia-conditioned media in response to IL-6 stimulation. These included diacylglycerophosphocholine, diacylglycerophospho-ethanolamine, and l-kynurenine, whereas N-methylethanolamine phosphate and formylanthranilate secretion increased in IL-6-stimulated neuronal cultures.

Diacylglycerophosphocholine and diacylglycerophosphoethanolamine belong to the class of glycerophospholipids (GPLs), an inactive pool from which bioactive lipids are synthesized [52,53]. Neuronal-astroglial membranes contain several classes of GPLs, which constitute the membrane backbone and define membrane properties such as fluidity and ion permeability [52,54]. GPLs and the complementary bioactive lipid breakdown products have been shown to modulate membrane excitability, monoaminergic neurotransmission, and brain development [39,55]. Recent evidence suggests that GPL metabolism is a critical disturbance across multiple brain diseases, as degradation of GPLs by phospholipase $A_2$ can release arachidonic acid and docosahexaenoic acid. The subsequent peroxidation and enzymatic processing of these long-chain polyunsaturated fatty acids produces multiple bioactive lipid mediators, all closely associated with neuronal metabolic pathways involved in the pathophysiology of major depression, schizophrenia, and Alzheimer's disease [56-58]. Furthermore, plasma phospholipid concentrations have been demonstrated as predictive of memory impairment in elderly adults [59].

In addition to altered GPL metabolism, exposure to IL-6 demonstrates a significant effect on at least two metabolites within the tryptophan-kynurenine pathway. L-kynurenine is the metabolite whose breakdown leads to the generation of bioactive kynurenic and quinolinic acids, which act on the glutamatergic and nicotinic neurotransmission as antagonists and agonists, respectively [60-62]. The tryptophan-kynurenine pathway is intricately linked to inflammatory cytokines through the enzyme of indoleamine 2,3-dioxygenase (IDO), which is the rate limiting step in the degradation of tryptophan into kynurenine and the subsequent formation of downstream metabolites [63,64]. Tryptophan metabolites demonstrate immunomodulatory effects, with increased tryptophan metabolites leading to apoptosis and cell cycle arrest and induction of T regulatory cells [65,66]. Neuroimaging, biomarker, and animal model studies all indicate that disturbances in the tryptophan-kynurenine pathway are a critical pathophysiological event in major depression [38,64,67] and potentially other neuropsychiatric disorders [41,62,68,69]. Our observation of altered kynurenic acid and formylanthranilate levels (both critical components of the tryptophan-kynurenine pathway) in response to IL-6 stimulation suggests that our system is relevant for studying brain disease-related processes and allows future dissection of this molecular pathway under controlled stimulation of astrocytes and neurons. Furthermore, our experimental system has the capability to dissect the secretory interplay between different brain cell types and immune cells, including (but not limited to) astroglia, neurons, microglia, and ependymal, endothelial, and T cells, as well as the study of the blood-brain barrier [70].

Based on our results, we hypothesize that the previously described detrimental effects of IL-6 on developing

neurons are at least partially due to the response of astroglia to IL-6, resulting in an altered exometabolomic profile, which in turn has a damaging effect on neurons. We intend to investigate this hypothesis further in follow-up, mechanistic studies which would test the effects the IL-6-induced astroglial exometabolome has on neuronal differentiation, growth, and synapse formation. This investigation, coupled with precise identification and testing the effects of individual metabolites, would lead to a better understanding of neurotoxic and neuroprotective processes that might occur in the developing brain. Future experiments will also encompass defining exometabolomic changes, responses, and interplay between various subclasses of neurons and across the various brain regions, leading to three-dimensional *in vitro* modeling of the brain.

It is also noteworthy that IL-6 response is quite conserved across species [71-73] and that the general CNS development in rodents is governed by the same basic principles as in humans [74]. Thus, we believe that our findings, obtained on developing mouse neurons, are also relevant for human conditions such as schizophrenia and autism. This view is also underscored by human disease findings of elevated cytokines in schizophrenia and autism [6,7,10], as well as the critical role of IL-6 in maternal immune activation models [8-10].

## Conclusions

In summary, our studies utilize microfluidic technology with a superb cell-to-media volume ratio, which is ideally suited for analysis of cell-type-specific metabolic signatures. We find that 1) developing neurons have lower metabolic activity at baseline than astroglia, which show strong production of metabolites; 2) both neurons and astroglia respond to IL-6 exposure in a cell-type-specific fashion; 3) with IL-6 stimulation of each cell type, metabolite production predominantly increases for the astrocytes as compared to sham-treated cells, but decreases for neurons; and 4) disturbances in glycerophospholipid metabolism and tryptophan/kynurenine metabolite secretion are two important mechanisms by which IL-6 might affect the developing nervous system.

## Additional files

**Additional file 1: Energy spectra for mass 156.04.** Low (top) and high (bottom) energy spectra for mass 156.04, putatively identified as n-methylethanolamine phosphate. The fragmentation spectrum is mobility selected to isolate only product ions for this mass.

**Additional file 2: Energy spectra for mass 209.10.** Low (top) and high (bottom) energy spectra for mass 209.10, putatively identified as kynurenine. The fragmentation spectrum is mobility selected to isolate only product ions for this mass.

**Additional file 3: Energy spectra for mass 166.05.** Low (top) and high (bottom) energy spectra for mass 166.05, putatively identified as formylanthranilate. The fragmentation spectrum is mobility selected to isolate only product ions for this mass.

**Additional file 4: Energy spectra for mass 732.55.** Low (top) and high (bottom) energy spectra for mass 732.55, a fragment of 760.59 and putatively identified as a phosphatidylcholine (PC). The fragmentation spectrum is mobility selected to isolate only product ions for this mass. A characteristic fragment ion of PCs is an ion at m/z 184, which is the phosphatidylcholine head group (structure shown above). The above structure is ONLY an example of the structure of PCs.

**Additional file 5: Energy spectra for mass 768.56.** Low (top) and high (bottom) energy spectra for mass 768.56, putatively identified as a phosphatidylethanolamine (PE). The fragmentation spectrum is mobility selected to isolate only product ions for this mass. A characteristic fragment ion of PEs is the neutral loss of 141, which is the ethanolaminephosphate head group (structure shown above). The above structure is ONLY an example of the structure of PEs.

**Additional file 6: Dataset 1.** Baseline astroglia and neurons, secreted and consumed – all data.

**Additional file 7: Dataset 2.** Neuron versus glial baseline – all data.

**Additional file 8: Dataset 3.** Effect of interleukin-6 – all data.

**Additional file 9: Exometabolomic response of neurons and glia to IL-6 stimulation.** Abbreviations: m/z, mass-to-charge ratio; RT, retention time; NIL6, neurons + IL-6; GIL6, glia + IL-6 stimulation; EIL6, empty chamber + IL-6 containing media; ALR, average Log2 ratio; *P* val, *P* value.

### Abbreviations

AA: arachidonic acid; ALR: average logarithmic ratio; BEH: ethylene bridged hybrid; CNS: central nervous system; DHA: docosahexaenoic acid; EPA: eicosapentaenoic acid; GFAP: glial fibrillary acidic protein; GPL: glycerophospholipid; HBSS: Hank's balanced salt solution; IDO: indoleamine 2,3-dioxygenase; IL-6: interleukin-6; IM-MS: ion mobility - mass spectrometry; LC: liquid chromatography; LCPUFA: long-chain polyunsaturated fatty acid; LPS: lipopolysaccharide; MEM: minimum essential medium; MIA: maternal immune activation; MS: mass spectrometry; $MS^E$: data-independent acquisition mass spectrometry; NB: neural basal; PCA: principal component analysis; PDMS: polydimethylsiloxane; Polyl:C: polyinosinic:polycytidylic acid; RT: retention time; UPLC: ultra-performance liquid chromatography; UPLC-IM-MS: ultra-performance liquid chromatography - ion mobility - mass spectrometry.

### Competing interests

The authors declare that they have no competing interests.

### Authors' contributions

JAB, JAM, JPW, and KM designed the study; JAB designed and executed experiments in bioreactors; SDS and CRG designed and executed analyses methods and UPLC IM-MS methods; JAB and SDS performed research; BB, LY, and DL contributed new analytic tools; KAG analyzed data; JAB, SDS, CRG, JAM, JPW, and KM analyzed, integrated, and interpreted data; JAB, SDS, CRG, and KM wrote the manuscript; and BB, LY, KAG, DL, JAM, and JPW edited the manuscript. All authors read and approved the final manuscript.

### Acknowledgements

This work and the preparation of the manuscript were supported in part by grants from the National Institutes of Health: R01 MH079299 (NIMH) to KM, UH2 TR000491 (NCATS and the NIH Common Fund) to JPW, and P30 HD15052 (NICHD) awarded to the Vanderbilt Kennedy Center for Research on Human Development; JAB is supported by 2T32MH065215-11 (NIMH). A portion of the work was also funded by a Vanderbilt University Discovery Grant to JPW. The content of this manuscript is solely the responsibility of the authors and does not necessarily represent the official views of the funding agencies and organizations. The funding agencies and organizations had no role in the design, collection, analysis, and interpretation of data, nor were they involved in the writing of the manuscript and the decision to submit it for publication. We appreciate the support of the Vanderbilt Institute for Integrative Biosystems Research and Education (VIIBRE) and the Vanderbilt Institute of Chemical Biology, and thank Allison Price of VIIBRE for editing and providing valuable comments on the manuscript.

**Author details**
[1]Department of Psychiatry, 465 21st Avenue South, Vanderbilt University, Nashville, TN 37232, USA. [2]Vanderbilt Institute for Integrative Biosystems Research and Education, 6809 Stevenson Center, Vanderbilt University, Nashville, TN 37235, USA. [3]Department of Physics and Astronomy, 6301 Stevenson Center, Vanderbilt University, Nashville, TN 37235, USA. [4]Department of Chemistry, 5421 Stevenson Center, Vanderbilt University, Nashville, TN 37235, USA. [5]Department of Mechanical Engineering, 333 Olin Hall, Vanderbilt University, Nashville, TN 37235, USA. [6]Department of Biomedical Engineering, 5824 Stevenson Center, Vanderbilt University, Nashville 37235, TN, USA. [7]Department of Molecular Physiology and Biophysics, 702 Light Hall, Vanderbilt University, Nashville, TN 37232, USA. [8]Vanderbilt Kennedy Center for Research on Human Development, 110 Magnolia Circle, Vanderbilt University, Nashville, TN 37203, USA. [9]Department of Psychiatry, University of Szeged, 6725 Szeged, Hungary.

Received: 25 August 2014 Accepted: 11 October 2014
Published online: 06 November 2014

**References**

1. Arion D, Unger T, Lewis DA, Levitt P, Mirnics K: **Molecular evidence for increased expression of genes related to immune and chaperone function in the prefrontal cortex in schizophrenia.** *Biol Psychiatry* 2007, **62:**711–721.
2. Voineagu I, Wang X, Johnston P, Lowe JK, Tian Y, Horvath S, Mill J, Cantor RM, Blencowe BJ, Geschwind DH: **Transcriptomic analysis of autistic brain reveals convergent molecular pathology.** *Nature* 2011, **474:**380–384.
3. Garbett K, Ebert PJ, Mitchell A, Lintas C, Manzi B, Mirnics K, Persico AM: **Immune transcriptome alterations in the temporal cortex of subjects with autism.** *Neurobiol Dis* 2008, **30:**303–311.
4. Shelton RC, Claiborne J, Sidoryk-Wegrzynowicz M, Reddy R, Aschner M, Lewis DA, Mirnics K: **Altered expression of genes involved in inflammation and apoptosis in frontal cortex in major depression.** *Mol Psychiatry* 2010, **16:**751–762.
5. Ganguly D, Haak S, Sisirak V, Reizis B: **The role of dendritic cells in autoimmunity.** *Nat Rev Immunol* 2013, **13:**566–577.
6. Horvath S, Mirnics K: **Immune system disturbances in schizophrenia.** *Biol Psychiatry* 2014, **75:**316–323.
7. Michel M, Schmidt MJ, Mirnics K: **Immune system gene dysregulation in autism and schizophrenia.** *Dev Neurobiol* 2012, **72:**1277–1287.
8. Shi L, Fatemi SH, Sidwell RW, Patterson PH: **Maternal influenza infection causes marked behavioral and pharmacological changes in the offspring.** *J Neurosci* 2003, **23:**297–302.
9. Hsiao EY, McBride SW, Chow J, Mazmanian SK, Patterson PH: **Modeling an autism risk factor in mice leads to permanent immune dysregulation.** *Proc Natl Acad Sci U S A* 2012, **109:**12776–12781.
10. Shi L, Tu N, Patterson PH: **Maternal influenza infection is likely to alter fetal brain development indirectly: the virus is not detected in the fetus.** *Int J Dev Neurosci* 2005, **23:**299–305.
11. Patterson PH: **Immune involvement in schizophrenia and autism: etiology, pathology and animal models.** *Behav Brain Res* 2009, **204:**313–321.
12. Garbett KA, Hsiao EY, Kalman S, Patterson PH, Mirnics K: **Effects of maternal immune activation on gene expression patterns in the fetal brain.** *Transl Psychiatry* 2012, **2:**e98.
13. Smith SE, Li J, Garbett K, Mirnics K, Patterson PH: **Maternal immune activation alters fetal brain development through interleukin-6.** *J Neurosci* 2007, **27:**10695–10702.
14. Hsiao EY, Patterson PH: **Activation of the maternal immune system induces endocrine changes in the placenta via IL-6.** *Brain Behav Immun* 2011, **25:**604–615.
15. Erta M, Quintana A, Hidalgo J: **Interleukin-6, a major cytokine in the central nervous system.** *Int J Biol Sci* 2012, **8:**1254–1266.
16. Spooren A, Kolmus K, Laureys G, Clinckers R, De Keyser J, Haegeman G, Gerlo S: **Interleukin-6, a mental cytokine.** *Brain Res Rev* 2011, **67:**157–183.
17. Stolp HB: **Neuropoietic cytokines in normal brain development and neurodevelopmental disorders.** *Mol Cell Neurosci* 2012, **53:**63–68.
18. Wikswo JP, Curtis EL, Eagleton ZE, Evans BC, Kole A, Hofmeister LH, Matloff WJ: **Scaling and systems biology for integrating multiple organs-on-a-chip.** *Lab Chip* 2013, **13:**3496–3511.
19. Faley S, Seale K, Hughey J, Schaffer DK, VanCompernolle S, McKinney B, Baudenbacher F, Unutmaz D, Wikswo JP: **Microfluidic platform for real-time signaling analysis of multiple single T cells in parallel.** *Lab Chip* 2008, **8:**1700–1712.
20. Enders JR, Marasco CC, Wikswo JP, McLean JA: **A dual-column solid phase extraction strategy for online collection and preparation of continuously flowing effluent streams for mass spectrometry.** *Anal Chem* 2012, **84:**8467–8474.
21. Brown JA, Diggs-Andrews KA, Gianino SM, Gutmann DH: **Neurofibromatosis-1 heterozygosity impairs CNS neuronal morphology in a cAMP/PKA/ROCK-dependent manner.** *Mol Cell Neurosci* 2011, **49:**13–22.
22. Clarris HJ, Nurcombe V, Small DH, Beyreuther K, Masters CL: **Secretion of nerve growth factor from septum stimulates neurite outgrowth and release of the amyloid protein precursor of Alzheimer's disease from hippocampal explants.** *J Neurosci Res* 1994, **38:**248–258.
23. Kerrison JB, Zack DJ: **Neurite outgrowth in retinal ganglion cell culture.** *Methods Mol Biol* 2007, **356:**427–434.
24. Dugan LL, Kim JS, Zhang Y, Bart RD, Sun Y, Holtzman DM, Gutmann DH: **Differential effects of cAMP in neurons and astrocytes.** *Role of B-raf J Biol Chem* 1999, **274:**25842–25848.
25. Sandsmark DK, Zhang H, Hegedus B, Pelletier CL, Weber JD, Gutmann DH: **Nucleophosmin mediates mammalian target of rapamycin-dependent actin cytoskeleton dynamics and proliferation in neurofibromin-deficient astrocytes.** *Cancer Res* 2007, **67:**4790–4799.
26. Dugan JP, Stratton A, Riley HP, Farmer WT, Mastick GS: **Midbrain dopaminergic axons are guided longitudinally through the diencephalon by Slit/Robo signals.** *Mol Cell Neurosci* 2011, **46:**347–356.
27. McDonald JC, Whitesides GM: **Poly(dimethylsiloxane) as a material for fabricating microfluidic devices.** *Acc Chem Res* 2002, **35:**491–499.
28. Whitesides GM, Ostuni E, Takayama S, Jiang X, Ingber DE: **Soft lithography in biology and biochemistry.** *Annu Rev Biomed Eng* 2001, **3:**335–373.
29. Shi M, Majumdar D, Gao Y, Brewer BM, Goodwin CR, McLean JA, Li D, Webb DJ: **Glia co-culture with neurons in microfluidic platforms promotes the formation and stabilization of synaptic contacts.** *Lab Chip* 2013, **13:**3008–3021.
30. Gao Y, Majumdar D, Jovanovic B, Shaifer C, Lin PC, Zijlstra A, Webb DJ, Li D: **A versatile valve-enabled microfluidic cell co-culture platform and demonstration of its applications to neurobiology and cancer biology.** *Biomed Microdevices* 2011, **13:**539–548.
31. Brewer BM, Shi M, Edd JF, Webb DJ, Li D: **A microfluidic cell co-culture platform with a liquid fluorocarbon separator.** *Biomed Microdevices* 2014, **16**(2):311–323.
32. Kuehn H, Liberzon A, Reich M, Mesirov JP: **Using GenePattern for gene expression analysis.** *Curr Protoc Bioinformatics* 2008, **Chapter 7:**Unit 7 12.
33. Kessner D, Chambers M, Burke R, Agus D, Mallick P: **ProteoWizard: open source software for rapid proteomics tools development.** *Bioinformatics* 2008, **24:**2534–2536.
34. Smith CA, O'Maille G, Want EJ, Qin C, Trauger SA, Brandon TR, Custodio DE, Abagyan R, Siuzdak G: **METLIN: a metabolite mass spectral database.** *Ther Drug Monit* 2005, **27:**747–751.
35. Wishart DS: **Current progress in computational metabolomics.** *Brief Bioinform* 2007, **8:**279–293.
36. Sud M, Fahy E, Cotter D, Brown A, Dennis EA, Glass CK, Merrill AH Jr, Murphy RC, Raetz CR, Russell DW, Subramaniam S: **LMSD: LIPID MAPS structure database.** *Nucleic Acids Res* 2007, **35:**D527–D532.
37. da Costa KA, Rai KS, Craciunescu CN, Parikh K, Mehedint MG, Sanders LM, McLean-Pottinger A, Zeisel SH: **Dietary docosahexaenoic acid supplementation modulates hippocampal development in the Pemt−/− mouse.** *J Biol Chem* 2010, **285:**1008–1015.
38. Myint AM, Schwarz MJ, Muller N: **The role of the kynurenine metabolism in major depression.** *J Neural Transm* 2011, **119:**245–251.
39. Janssen CI, Kiliaan AJ: **Long-chain polyunsaturated fatty acids (LCPUFA) from genesis to senescence: The influence of LCPUFA on neural development, aging, and neurodegeneration.** *Prog Lipid Res* 2013, **53C:**1–17.
40. Pfaffenseller B, Fries GR, Wollenhaupt-Aguiar B, Colpo GD, Stertz L, Panizzutti B, Magalhaes PV, Kapczinski F: **Neurotrophins, inflammation and oxidative stress as illness activity biomarkers in bipolar disorder.** *Expert Rev Neurother* 2013, **13:**827–842.
41. Muller N, Myint AM, Schwarz MJ: **Kynurenine pathway in schizophrenia: pathophysiological and therapeutic aspects.** *Curr Pharm Des* 2011, **17:**130–136.
42. McIntyre TM: **Bioactive oxidatively truncated phospholipids in inflammation and apoptosis: formation, targets, and inactivation.** *Biochim Biophys Acta* 2012, **1818:**2456–2464.

43. Schwarcz R, Pellicciari R: **Manipulation of brain kynurenines: glial targets, neuronal effects, and clinical opportunities.** *J Pharmacol Exp Ther* 2002, **303:**1–10.
44. Oxenkrug GF: **Tryptophan kynurenine metabolism as a common mediator of genetic and environmental impacts in major depressive disorder: the serotonin hypothesis revisited 40 years later.** *Isr J Psychiatry Relat Sci* 2010, **47:**56–63.
45. Johansson AS, Owe-Larsson B, Asp L, Kocki T, Adler M, Hetta J, Gardner R, Lundkvist GB, Urbanska EM, Karlsson H: **Activation of kynurenine pathway in ex vivo fibroblasts from patients with bipolar disorder or schizophrenia: cytokine challenge increases production of 3-hydroxykynurenine.** *J Psychiatr Res* 2013, **47:**1815–1823.
46. Doering LC (Ed): *Protocols for Neural Cell Culture.* 4th edition. New York: Humana Press; 2010.
47. Ji R, Tian S, Lu HJ, Lu Q, Zheng Y, Wang X, Ding J, Li Q: **TAM receptors affect adult brain neurogenesis by negative regulation of microglial cell activation.** *J Immunol* 2013, **191:**6165–6177.
48. Losino N, Waisman A, Solari C, Luzzani C, Espinosa DF, Sassone A, Muro AF, Miriuka S, Sevlever G, Baranao L, Guberman A: **EDA-containing fibronectin increases proliferation of embryonic stem cells.** *PLoS One* 2013, **8:**e80681.
49. Rao KM, Ma JY, Meighan T, Barger MW, Pack D, Vallyathan V: **Time course of gene expression of inflammatory mediators in rat lung after diesel exhaust particle exposure.** *Environ Health Perspect* 2005, **113:**612–617.
50. Wei F, Guo W, Zou S, Ren K, Dubner R: **Supraspinal glial-neuronal interactions contribute to descending pain facilitation.** *J Neurosci* 2008, **28:**10482–10495.
51. Polazzi E, Contestabile A: **Neuron-conditioned media differentially affect the survival of activated or unstimulated microglia: evidence for neuronal control on apoptotic elimination of activated microglia.** *J Neuropathol Exp Neurol* 2003, **62:**351–362.
52. Morell P, Ousley AH: **Metabolic turnover of myelin glycerophospholipids.** *Neurochem Res* 1994, **19:**967–974.
53. Lee C, Fisher SK, Agranoff BW, Hajra AK: **Quantitative analysis of molecular species of diacylglycerol and phosphatidate formed upon muscarinic receptor activation of human SK-N-SH neuroblastoma cells.** *J Biol Chem* 1991, **266:**22837–22846.
54. Frisardi V, Panza F, Seripa D, Farooqui T, Farooqui AA: **Glycerophospholipids and glycerophospholipid-derived lipid mediators: a complex meshwork in Alzheimer's disease pathology.** *Prog Lipid Res* 2011, **50:**313–330.
55. Chen C, Bazan NG: **Lipid signaling: sleep, synaptic plasticity, and neuroprotection.** *Prostaglandins Other Lipid Mediat* 2005, **77:**65–76.
56. Lopresti AL, Maker GL, Hood SD, Drummond PD: **A review of peripheral biomarkers in major depression: the potential of inflammatory and oxidative stress biomarkers.** *Prog Neuropsychopharmacol Biol Psychiatry* 2013, **48:**102–111.
57. Najjar S, Pearlman DM, Hirsch S, Friedman K, Strange J, Reidy J, Khoukaz M, Ferrell RB, Devinsky O, Najjar A, Zagzag D: **Brain biopsy findings link major depressive disorder to neuroinflammation, oxidative stress, and neurovascular dysfunction: a case report.** *Biol Psychiatry* 2014, **75:**e23–e26.
58. Wu JQ, Kosten TR, Zhang XY: **Free radicals, antioxidant defense systems, and schizophrenia.** *Prog Neuropsychopharmacol Biol Psychiatry* 2013, **46:**200–206.
59. Mapstone M, Cheema AK, Fiandaca MS, Zhong X, Mhyre TR, Federoff HJ: **Plasma phospholipids identify antecedent memory impairment in older adults.** *Nat Med* 2014, **20**(4):415–418.
60. Stone TW: **Kynurenic acid antagonists and kynurenine pathway inhibitors.** *Expert Opin Investig Drugs* 2001, **10:**633–645.
61. Freese A, Swartz KJ, During MJ, Martin JB: **Kynurenine metabolites of tryptophan: implications for neurologic diseases.** *Neurology* 1990, **40:**691–695.
62. Stone TW, Forrest CM, Darlington LG: **Kynurenine pathway inhibition as a therapeutic strategy for neuroprotection.** *FEBS J* 2012, **279:**1386–1397.
63. Dantzer R, O'Connor JC, Lawson MA, Kelley KW: **Inflammation-associated depression: from serotonin to kynurenine.** *Psychoneuroendocrinology* 2010, **36:**426–436.
64. Myint AM, Bondy B, Baghai TC, Eser D, Nothdurfter C, Schule C, Zill P, Muller N, Rupprecht R, Schwarz MJ: **Tryptophan metabolism and immunogenetics in major depression: a role for interferon-gamma gene.** *Brain Behav Immun* 2013, **31:**128–133.
65. Munn DH, Mellor AL: **Indoleamine 2,3-dioxygenase and tumor-induced tolerance.** *J Clin Invest* 2007, **117:**1147–1154.
66. Jain A, Munn LL: **Biomimetic postcapillary expansions for enhancing rare blood cell separation on a microfluidic chip.** *Lab Chip* 2011, **11:**2941–2947.
67. Oxenkrug G: **Serotonin-kynurenine hypothesis of depression: historical overview and recent developments.** *Curr Drug Targets* 2013, **14:**514–521.
68. Myint AM: **Kynurenines: from the perspective of major psychiatric disorders.** *FEBS J* 2012, **279:**1375–1385.
69. Plangar I, Zadori D, Klivenyi P, Toldi J, Vecsei L: **Targeting the kynurenine pathway-related alterations in Alzheimer's disease: a future therapeutic strategy.** *J Alzheimers Dis* 2011, **24**(Suppl 2):199–209.
70. Alcendor DJ, Block FE III, Cliffel DE, Daniels JS, Ellacott KL, Goodwin CR, Hofmeister LH, Li D, Markov DA, May JC, McCawley LJ, McLaughlin B, McLean JA, Niswender KD, Pensabene V, Seale KT, Sherrod SD, Sung HJ, Tabb DL, Webb DJ, Wikswo JP: **Neurovascular unit on a chip: implications for translational applications.** *Stem Cell Res Ther* 2013, **4**(Suppl 1):S18.
71. Burton MD, Sparkman NL, Johnson RW: **Inhibition of interleukin-6 trans-signaling in the brain facilitates recovery from lipopolysaccharide-induced sickness behavior.** *J Neuroinflammation* 2011, **8:**54.
72. Campbell IL, Erta M, Lim SL, Frausto R, May U, Rose-John S, Scheller J, Hidalgo J: **Trans-signaling is a dominant mechanism for the pathogenic actions of interleukin-6 in the brain.** *J Neurosci* 2014, **34:**2503–2513.
73. Semple BD, Blomgren K, Gimlin K, Ferriero DM, Noble-Haeusslein LJ: **Brain development in rodents and humans: identifying benchmarks of maturation and vulnerability to injury across species.** *Prog Neurobiol* 2013, **106–107:**1–16.
74. Trapero I, Cauli O: **Interleukin 6 and cognitive dysfunction.** *Metab Brain Dis* 2014, **29:**593–608.

doi:10.1186/s12974-014-0183-6
**Cite this article as:** Brown *et al.*: Metabolic consequences of interleukin-6 challenge in developing neurons and astroglia. *Journal of Neuroinflammation* 2014 **11**:183.